Investigation into the Biological Impact of Block Size on Cathepsin S-degradable HPMA Copolymers

Wei Fan[†,‡,§], **Wenting Zhang**[†,‡,§], **Yinnong Jia**[†,‡], **Susan K. Brusnahan**[†,‡], and **Jered C. Garrison**[*,†,‡,∥,⊥]

[†]Department of Pharmaceutical Sciences, College of Pharmacy, University of Nebraska Medical Center, Omaha, Nebraska 985830, United States

[‡]Center for Drug Delivery and Nanomedicine, University of Nebraska Medical Center, Omaha, Nebraska 985830, United States

[∥]Department of Biochemistry and Molecular Biology, College of Medicine, University of Nebraska Medical Center, Omaha, Nebraska 985830, United States

[⊥]Eppley Cancer Center, University of Nebraska Medical Center, Omaha, Nebraska 985830, United States

Abstract

N-(2-hydroxypropyl)methacrylamide (HPMA) copolymers have been studied as an efficient carrier for drug delivery and tumor imaging. However, as with many macromolecular platforms, the substantial accumulation of HPMA copolymer by the mononuclear phagocyte system (MPS)-associated tissues, such as the blood, liver and spleen, has inhibited its clinical translation. Our laboratory is pursuing approaches to improve the diagnostic and radiotherapeutic effectiveness of HPMA copolymers by reducing the non-target accumulation. Specifically, we have been investigating the use of a cathepsin S (Cat S)-cleavable peptidic linkers to degrade multi-block HPMA copolymers to increase MPS-associated tissue clearance. In this study, we further our investigation into this area by exploring the impact of copolymer block size on the biological performance of Cat S-degradable HPMA copolymers. Using a variety of *in vitro* and *in vivo* techniques, including dual labeling of the copolymer and peptide components, we investigated the constructs using HPAC pancreatic ductal adenocarcinoma models. The smaller copolymer block size (S-CMP) demonstrated significantly faster Cat S cleavage kinetics relative to the larger system (L-CMP). Confocal microscopy demonstrated that both constructs could be much more

[*]**Corresponding Author**: jcgarrison@unmc.edu.
**Author Contributions**: W.F. and W.Z. contributed equally to the work.

Notes

efficiently internalized by human monocyte-differentiated macrophage (hMDM) compared to HPAC cells. In the biodistribution studies, the multi-block copolymers with a smaller block size exhibited faster clearance and lower non-target retention while still achieving good tumor targeting and retention. Based on the radioisotopic ratios, fragmentation and clearance of the copolymer constructs was higher in the liver compared to the spleen and tumor. Overall, these results indicate that block size plays an important role in the biological performance of Cat S-degradable polymeric constructs.

Graphical abstract
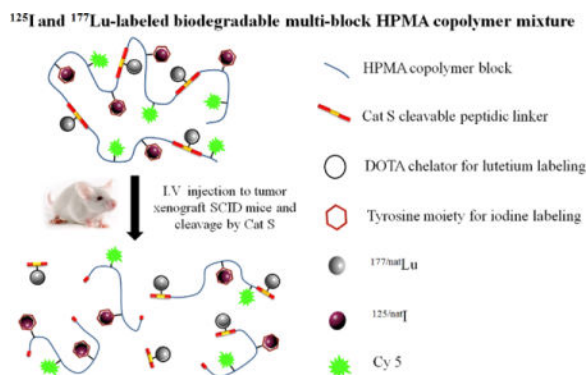
Keywords

Cathepsin S; HPMA; Dual-isotope labeling; Mononuclear phagocyte system; Pancreatic cancer

INTRODUCTION

Diagnostic imaging is a crucial tool in the effective management of most cancers.[1] Nuclear imaging techniques, such as single-photon emission computed tomography (SPECT) and positron emission tomography (PET), have been a central part of the available diagnostic apparatuses to detect, stage and monitor cancer progression.[2, 3] The development of radiotracers utilized for these nuclear imaging modalities have utilized carriers with molecular weights that range from small molecules to antibodies.[4–6] Despite the many advantages of nanomedicine platforms, such as increased drug payload, multi-functional capabilities and passive targeting through the enhanced permeability and retention (EPR) effect, relatively little effort over the years has focused on the development of radiotracers based on these systems.[7, 8] This has largely been due to the uptake and retention of the platforms in non-target tissues (e.g., blood, liver and spleen) associated with the MPS,[9] which results in relatively poor tumor-to-non-target ratios and significantly diminished diagnostic capabilities.

N-(2-hydroxypropyl)methacrylamide (HPMA) copolymers have been a well-known and well-validated polymeric drug carrier for the delivery of chemotherapeutics,[10] but have also been investigated as a potential platform for the development of nuclear imaging and radiotherapeutic agents.[11–14] Despite the increased tumor targeting capabilities of larger, longer-circulating HPMA copolymers, much of the reported SPECT or PET agent

development to date has centered on the utilization of HPMA copolymers that are lower than the renal excretion threshold, ~ 45 kDa, to limit MPS uptake and retention. Our laboratory has been investigating the exploitation of a protease, Cat S, which is highly expressed in the phagocytic cells constituting the MPS in order to lower the non-target retention of radiolabeled polymeric drug carriers.[15–17] The incorporation of Cat S-susceptible peptide linkers into the backbone of the HPMA copolymers leads to significant decreases in the retention of these agents in MPS-associated tissues, resulting in enhanced imaging contrast. Based on the *in vitro* studies to date, the *in vivo* mechanism of the increased non-target clearance of these Cat S-degradable HPMA copolymers is likely due to fragmentation and enhanced clearance of the smaller polymeric blocks.[17]

Currently, the impact of the molecular weight of the copolymer blocks on the biological performance of Cat S-degradable HPMA copolymers is not known. Understanding the structural factors effecting the *in vivo* fate of the copolymer and gaining insight into the *in vivo* clearance mechanism(s) of these agents is crucial for the rational improvement of this approach. In the current study, our laboratory continues the exploration of the structure-activity relationship and clearance mechanism of these Cat S-degradable HPMA copolymers (Figure 1). Herein, we discuss the synthesis of the multi-block HPMA copolymers constituted from small (17.4 kDa) and large (32.9 kDa) block sizes and explore the impact of this modification on the *in vitro* and *in vivo* performance of these agents using pancreatic cancer models. Additionally, using dual-isotope labels to simultaneously monitor peptide and copolymer concentrations, the tissue specific rates of *in vivo* fragmentation and clearance were examined.

EXPERIMENTAL SECTION

Materials

Reagents—All solvents used for reaction and silica gel purification were ACS grade and purchased from Fisher Scientific. Acetonitrile was HPLC grade and purchased from Fisher Scientific. Water was deionized by Millipore® Milli Q Biocell Ultrapure Water System before use. Trifluoroacetic acid (TFA) was purchased from Fisher Scientific. 6-Maleimidohexanoic acid was purchased from Alfa Aesar. 1-[(1-(Cyano-2-ethoxy-2-oxoethylideneaminooxy) dimethylaminomorpholino)] uronium hexafluorophosphate (COMU), Fmoc-protected amino acids and tris(2-carboxyethyl) phosphine (TCEP) were purchased from NovaBiochem. N-(2-Hydroxypropyl)methacrylamide was purchased from Polysciences. Tyr-MA and DOTA-NHS were synthesized according to reported methods.[18, 19] Dulbecco's Modified Eagle Medium (DMEM), and phosphate buffered saline (PBS) were obtained from Fisher Scientific. $^{177}LuCl_3$ and $Na^{125}I$ were purchased from PerkinElmer. The human pancreatic adenocarcinoma HPAC (CRL-2119) cell line was purchased from American Type Culture Collection. Human monocytes, human AB serum and rhM-CSF were provided by the UNMC Elutriation Core Facility. Matrigel® was obtained from BD Biosciences. Human AB serum, DMEM/Ham's F12 medium, L-glutamine and sodium pyruvate were obtained from Mediatech (U.S.). Fetal bovine serum (FBS) was purchased from Invitrogen/GIBCO (U.S.). L-glutamine, LysoTracker® Red DND-99 and NucBlue® Live ReadyProbe® reagent were purchased from Thermo Fisher

Scientific. Five week old female SCID mice were purchased from Charles River Laboratories. All procedures utilizing animals conform to the Guide for the Care and Use of Laboratory Animals of the National Institutes of Health, and were approved by the Institutional Animal Care and Use Committee at the University of Nebraska Medical Center.

Instrumentation—Peptides were synthesized by solid phase peptide synthesis (SPPS) on a Liberty microwave peptide synthesizer from CEM. A Waters e2695 system equipped with a Waters 2489 absorption detector and a Waters Qtof Micro electrospray ionization mass spectrometer was used to perform high performance liquid chromatography/mass spectrometry analyses. ^{1}H NMR spectrums were recorded on a Bruker Avance-III HD 600 MHz instrument using euterium oxide as the solvent. A Phenomenex Jupiter C12 Proteo 250 10 mm semiprep column was used for the purification of bulk amounts of peptides. A Viscotek TDA max system equipped with Shodex Asahipak GF-510 HQ GPC column was used for HPMA copolymer molecular weight and size measurements. A Sephadex® LH-20 size exclusion resin obtained from GE HealthCare was used for bulk chromatographic separations. Evaluation and purification of radiolabeled copolymers were performed on a Waters 1515 binary pump equipped with a Waters 2489 absorption detector and a Bioscan Flow Count radiometric detector system using an Agilent PL aquagel-OH MIXED-H Gel Permation Chromatography (GPC) column. Lab-Tek chambered #1.0 borosilicate coverglass disks (4 well) were used for confocal cell imaging. Confocal microscopy images were taken on a Leica LSM 510 META Microscope equipped with an argon laser. Gamma decay detection of ^{177}Lu and ^{125}I dual-labeled polymer conjugates for biodistribution studies was accomplished using a NaI (Tl) well detector constructed by AlphaSpectra Inc.

Synthesis of copolymers

Synthesis of telechelic-block HPMA copolymer (S-BP and L-BP)—CTA **1** and initiator **2** were added to a solution containing 1.0 M HPMA monomer, 15 mM Tyr-AM and 5 mM APMA in 500 μL of 33% dioxane in Water. The molar ratio between monomers, CTA and initiator were set as 100:1:1.15 for S-BP. The solution was transferred to an ampoule and purged with nitrogen for 40 min. The polymerization was carried out in the sealed ampoule at 45 °C for 48 h and terminated by removal of heat and exposure to oxygen. The mixture was loaded on a LH-20 column to remove the unreacted low molecular weight compounds with methanol as the eluent to give a pink solid (65.5 mg, 87.6 %). For L-BP, the polymerization was carried out by the method described above using a ratio of 200:1:1.15 (monomers:CTA:initiator). Similarly, a light pink solid (62.0 mg, 82.9 %) was obtained.

Synthesis of deprotected S-BP and L-BP (S-dBP and L-dBP)—The copolymer block S-BP or L-BP (50 mg) was dissolved in 1 mL of methanol. To this solution, 100 μL of hexylamine was added. The solution was stirred for 2 h at room temperature and precipitated drop-wise into 50 mL of cold ether. The white precipitate was collected, dried and re-dissolved in 1 mL of deionized (DI) water. To this solution, TCEP (100 mol equiv relative to initial copolymer blocks) was added and the solution stirred overnight. The copolymer blocks were purified using a LH-20 column with methanol as the eluent. The purified solution was evaporated to dryness to obtain S-dBP (44.1 mg, 88.3 %) or L-dBP (42.6 mg,

85.2 %) as white solid and the content of tyrosine moieties in the copolymer was determined by UV absorbance at 280 nm.

Telechelic extension and fractionation of multi-block HPMA copolymers (S-MP and L-MP)—The HPMA copolymer block (10 mg) and the DOTA conjugated peptide linker (3.4 mg) were dissolved in 300 μL of PBS buffer (pH = 6.8). The mixture was purged with nitrogen for 30 min and stirred at 50 °C for 48 h. The solution was filtered through a 0.22 μm filter and fractionated on an Asahipak GF-510 HQ column using 40% acetonitrile and 60% PBS as the eluent. For L-MP, eluent from 5 mL to 6.5 mL was collected while the eluate from 5.3 mL to 6.8 mL was collected for S-MP. The solutions were concentrated in vacuo, desalted by using an Amicon ultrafiltration cell with a 10 kDa MWCO membrane, and lyophilized to give S-MP (2.87 mg, 17.1%) and L-MP (2.32 mg, 15.8%).

Synthesis of Cy5-conjugated, multi-block HPMA copolymers (S-CMP and L-CMP)—The extended multi-block HPMA copolymers (2 mg) were dissolved in 350 μL of PBS buffer (pH = 8.0). To this solution was added Cy5-NHS ester (0.3 mg) in 150 μL of DMF. The mixture was kept in the dark and stirred for 24 h. The excess Cy5 was removed by dialysis using DI water. The purified solution was lyophilized and the Cy5 content was determined by UV absorbance at 650 nm. The yields for S-CMP and L-CMP were 90.7 % (1.83 mg) and 93.2% (1.87 mg), respectively.

Radiolabeling of multi-block HPMA copolymers

Iodine-labeling of multi-block HPMA copolymers—The iodination of the copolymers was carried out by oxidation of sodium iodide via Pierce® iodination beads. Briefly, one Pierce® iodination bead was first washed with 200 μL of $10 \times$ PBS buffer (pH = 6.25), followed by the addition of 200 μCi (7.4 MBq) of $Na^{125}I$ or 50 μg of $Na^{nat}I$ in 150 μL of $10 \times$ PBS buffer (pH = 6.8) and stirred for 10 min. S-CMP or L-CMP (0.2 mg) was dissolved in 50 μL of $10 \times$ PBS buffer (pH = 6.8), added to the mixture containing the iodination bead and allowed to stand for 2 h at room temperature. Purification of the iodinated copolymer was performed on an Agilent PL aquagel-OH MIXED-H GPC column using 40% acetonitrile in PBS as the eluent. The iodinated HPMA copolymers were identified and characterized by signals observed from a Waters 2489 UV detector (650 nm) and Bioscan flow count radiometric detector. For radioiodinated copolymers, the purified samples were collected and stored in a vial containing 5 mg of L-ascorbic acid to prevent radiolysis. The radiolabeled HPMA copolymers were desalted and concentrated by an Amicon ultrafiltration cell with a 10 kDa molecular weight cut off (MWCO) membrane before use.

Lutetium-labeling of multi-block HPMA copolymers—S-CMP or L-CMP (0.2 mg) was dissolved in 50 μL of DI water. To this solution was added 1 mCi (37 MBq) of $^{177}LuCl_3$ or 50 μg of $^{nat}LuCl_3$ and was subsequently heated to 90 °C for 45 min. The purification of the lutetium-labeled, multi-block HPMA copolymer was performed using an Agilent PL aquagel-OH MIXED-H GPC column with 40% acetonitrile in PBS as the eluent. The copolymers were identified by signals from a Waters 2489 UV detector (650 nm) and Bioscan flow count radiometric detector. The copolymer was collected in a tube containing 5

mg of L-ascorbic acid to prevent radiolysis. Before *in vitro* or *in vivo* studies were performed, the lutetium-labeled, multi-block HPMA copolymers were simultaneously desalted and concentrated as described above.

Evaluation of radioisotope distribution in the copolymers fractions

The mixture of 30 μCi (1.11 MBq) of ^{125}I-labeled and 150 μCi (5.56 MBq) of ^{177}Lu-labeled, HPMA copolymers (S-CMP or L-CMP) was diluted to a total volume of 150 μL using DI water. The mixture was injected into the radio-GPC-HPLC system, and the radioactivity of the HPMA copolymer was monitored by Bioscan flow count radiometric detector. The radioactivity peak associated with the dual-radiolabeled copolymer was equally split into 5 retention volume intervals, such as 5–5.3 mL, 5.3–5.6 mL, 5.6–5.9 mL, 5.9–6.2 mL and 6.2–6.5 mL for L-CMP or 5.3–5.6 mL, 5.6–5.9 mL, 5.9–6.2mL, 6.2–6.5 mL and 6.5–6.8 mL for S-CMP. Each fraction (10 μL) was analyzed by a NaI (Tl) well detector to determine the ^{125}I/^{177}Lu ratio.

Cell culture

Cells were plated on 6-well plate at a concentration of 10^6 cells in 1mL of culture medium or borosilicate coverglass disks at a concentration of 2×10^5 cells in 400 μL of culture medium. For macrophage differentiation, the DMEM medium contained 10% Human AB serum, 500 U rhM-CSF, 2mM L-glutamine and 1% penicillin/streptomycin. Medium was changed every 3 days for 7 days, at which time, visual confirmation of differentiation led to media replacement with the macrophage maintenance medium (differentiation media without the rhM-CSF). The HPAC cells were cultured in DMEM/Ham's F12 medium containing 5% FBS, 1.562 nM EGF, 14.3 mM sodium bicarbonate, 2.5 mM L-glutamine, 15 mM HEPES and 0.5 mM sodium pyruvate and supplemented with 0.350 mM insulin, 0.0625 mM transferrin and 0.110 mM hydrocortisone. Cells were maintained in a 37 °C humidified atmosphere with 5% CO_2.

In vitro cleavage and stability studies of multi-block HPMA copolymers

Cathepsin S Cleavage—Unlabeled or radiolabeled S-CMP or L-CMP was added to 100 μL of the cleavage buffer containing sodium acetate (50 mM), DTT (10 mM) and EDTA (1 mM) to make a concentration of 1 mg/mL or 10 μCi/mL (0.37 MBq/mL), respectively. To this mixture was added 250 ng of human Cat S and incubated for different time periods at 37 °C. At each time point, a 20 μL aliquot of the mixture was withdrawn and diluted with 90 μL of GPC eluent (40% acetonitrile in PBS). The 110 μL of sample was analyzed by a GPC-HPLC equipped with Waters 2489 UV detector and Malvern TDA system or radioactive-GPC-HPLC equipped with Waters 2489 UV detector and Bioscan flow count radiometric detector.

Cleavage by Human Monocyte Differentiated Macrophage (hMDM)—The cleavage studies of the multi-block copolymers by hMDM were performed by adding 100 μCi (3.7 MBq) of ^{125}I-labeled S-CMP or L-CMP to 6-well plate with used differentiation medium (1 mL) or the cells (with 1 mL of maintenance medium). After 12 h incubation, 150 μL of each medium was centrifuged and the supernatant was analyzed by the radio-GPC-HPLC.

Serum Stability Studies—The serum stability of the ^{125}I-labeled copolymers was determined by using GPC chromatography. Briefly, 5 μCi (0.19 MBq) of ^{125}I-labeled copolymers were incubated with 1 mL of human AB serum at 37 °C for 24 h. The mixture (500 μL) was dried under nitrogen flow and recovered in 100 μL of methanol, which was analyzed by radio-GPC-HPLC system.

Confocal microscopy

The multi-block HPMA copolymer (S-CMP or L-CMP) was dissolved in macrophage maintenance medium or medium utilized to culture HPAC cells to give a concentration of 0.2 mg/mL. Macrophages and HPAC cells were incubated with the multi-block HPMA copolymers containing medium (300 μL) for 12 h in a 37 °C humidified atmosphere with 5% CO_2. The cells were washed with fresh media after incubation, followed by the addition of LysoTracker Red DND-99 to a concentration of 150 nM and further incubation for 2 h. Hoechst 33342 was added in the media to stain the nuclei 15 min prior to imaging. The cells were washed with fresh medium and images were obtained using an excitation wavelength of 405 nm (blue excitation), 568 nm (red excitation) and 640 nm (cyan excitation).

Biodistribution studies

Five week old female SCID mice received subcutaneous injections of 5×10^6 HPAC cells suspended in Matrigel® into two flanks. When the tumor size reached 80 mm^3 (two weeks after injection), the mice were randomized into two groups and intravenously injected with 9 μCi (0.33 MBq) of ^{177}Lu-labeled and 3 μCi (1.11 MBq) of ^{125}I-labeled, multi-block HPMA copolymer mixture via tail vein. The mice were sacrificed and their tissues were excised at 4, 24, 72 and 144 h p.i. time points. The blood, tumor and excised tissues were weighed. The radioactivity for each sample was measured by gamma counter. The percentage injected dose per gram (%ID/g) for each isotope and their radioactivity ratios in different organs were calculated after decay correction.

Urine analysis of the ^{125}I-labeled multi-block HPMA copolymers

The ^{125}I-labeled HPMA multi-block HPMA copolymer (S-CMP or L-CMP) in PBS was intravenously administered to CF-1 mouse at a dose of 200 μCi (7.4 MBq). Urine was collected by fractions at 0 – 4 h, 4 – 72 h, and 72 – 144 h p.i. before the mice were sacrificed. The urine samples were centrifuged and the supernatants were analyzed using a radio-GPC-HPLC system with 40% acetonitrile in PBS as the eluent. The blood, heart, liver, muscle, and thyroid were excised and weighed. The radioactivity for each tissue sample was measured by a gamma counter.

RESULTS

Synthesis of copolymers

The overall synthesis of the multi-block copolymer systems is illustrated in Scheme 1. The copolymers targeted for synthesis are composed of HPMA, Tyr-AM and APMA monomers. To accommodate the planned synthetic route, the chain transfer agent cystamine-CTA **1** and initiator cystamine-ACVA **2** (Figure S1), synthesized as previously described,[17] were utilized in the RAFT polymerization reaction to yield HPMA copolymers with terminal thiol

functionality. The characteristics of these blocks and successive products are tabulated in Table 1. The small block copolymer (S-BP) and large block copolymer (L-BP) have weight average molecular weights (Mw) of 17.4 and 32.9 kDa, respectively, and polydispersities (PDI) of 1.03. Following the deprotection of the terminal thiols, the Tyr-AM composition of the copolymer blocks were measured and found to be 1.40 wt% and 1.36 wt% for S-dBP and L-dBP, respectively. Employing thiol-ene conjugation chemistry, a maleimide containing peptidic linker was synthesized to extend the copolymeric blocks into multi-block copolymers. The peptide linker is a quasi-symmetric peptide that contains a DOTA chelator and two P-M-G-L-P sequences, a known substrate for Cat S.[20] The synthesis and characterization of this linker is described in Scheme S1 and Figure S2, correspondingly.

The condensation reaction of the S-dBP and L-dBP with the peptide linker led to the formation of multi-block copolymers S-MP and L-MP, respectively. The GPC profiles of the copolymer blocks and the subsequent extension products are depicted in Figure 2. For both copolymer blocks, the extension reactions gave monomeric blocks with one and/or two peptides attached, dimeric blocks as well as trimer and higher order multimers. For the purpose of our studies, the trimer and higher order multimers were fractionally collected to give S-MP and L-MP with yields of 21.4 and 17.3 % and molecular weights of 91.3 and 139.3 kDa, correspondingly. Utilizing the molecular weights of the copolymer blocks, the peptide and the extended multi-block copolymers, estimates indicate an average of 4 – 5 DOTA moieties per multimer chain for both S-MP and L-MP.

In order to perform *in vitro* cell trafficking studies, Cy5 was subsequently conjugated to S-MP and L-MP, utilizing the free amine group of the incorporated APMA moieties. This addition resulted in the corresponding designation of S-CMP and L-CMP. The Cy5 content was measured and found to be 0.31 and 0.37 wt% for S-CMP and L-CMP, respectively. The characterization of S-CMP and L-CMP showed that the multi-block copolymers had an average molecular weight of 92.5 and 140.5 kDa with PDI of 1.34 and 1.39, correspondingly. The hydrodynamic radius of the multi-block copolymers is 7.21 and 9.85 nm, respectively, for S-CMP and L-CMP. Utilizing both constructs, the impact of the copolymer block size on the *in vitro* and *in vivo* behavior of the multi-block copolymer was investigated.

In vitro cleavage studies of S-CMP and L-CMP

The susceptibility of both S-CMP and L-CMP to Cat S degradation was examined longitudinally at 0, 1, 6 and 24 h time points. The GPC profiles of the reaction solutions are given in Figure 3. At the 0 h time point, all of the S-CMP and L-CMP gave elution volumes of approximately 6.8 and 6.2 mL, respectively. After exposure to Cat S for 1 h, both of the multi-block copolymers demonstrated a substantial shift toward higher elution volumes indicating a resulting decrease in molecular weight due to degradation. For the S-CMP, 83.8 % of the multi-block copolymer was degraded to a product with an elution volume of 7.9 mL, which correlated well to the elution volume of the monomeric block S-dBP (7.9 mL, Figure 2). By the 6 h time point, the degradation of S-CMP by Cat S was complete. Relative to S-CMP, the cleavage of L-CMP by Cat S was substantially slower with a mixture of monomeric, dimeric and multimeric copolymers present at the 1 h time point. Based on

the elution volume of L-dBP, only 30.1 % of the L-CMP had converted to the monomeric copolymer. However, by the 6 h time point, the L-CMP was almost completely degraded.

Radiolabeling of the copolymers

The design of the multi-block copolymers allowed for the selective labeling of both the copolymer and peptide components. Radioiodination of the copolymer can be easily accomplished through oxidative addition to the Tyr-AM functionality,[21] while the DOTA-incorporated peptide can be labeled using a variety of radiometals,[22] in this case lutetium-177 (^{177}Lu). For convenience, the labeling of the multi-block copolymers with the two radiolabels was performed separately and subsequently formulated together in the desired radioisotopic ratios. To minimize any differences in physiochemical properties, the multi-block copolymers were separately labeled with ^{177}LuCl$_3$ and Na^{nat}I or ^{nat}LuCl$_3$ and Na^{125}I. The radiolabeling yields for ^{177}Lu (with ^{nat}I) and ^{125}I (with ^{nat}Lu) with both S-CMP and L-CMP are listed in Figure S3. High isolated, radiochemical yields (> 82.5 %) were achieved for the ^{177}LuCl$_3$ labeling of both S-CMP and L-CMP, whereas relatively lower radiochemical yields (< 47.2 %) were obtained when labeling with Na^{125}I. In order to establish whether the radiolabels were homogenously distributed throughout the copolymers, a 5:1 mixture of ^{177}Lu- and ^{125}I-labeled S-CMP and L-CMP was fractionated by GPC-HPLC. Using gamma spectroscopy, the overlapped ^{177}Lu and ^{125}I signals were measured and deconvoluted according to the methodology and standard curve in Figure S4 and S5 (the details are described in the supporting information) to provide the ^{125}I/^{177}Lu ratios for each fraction, which are tabulated in Table S1. For both multi-block HPMA copolymers, the ^{125}I/^{177}Lu ratios for the five continuous fractions were consistent and ranged from 0.27 – 0.31. A slight trend toward higher ^{125}I/^{177}Lu ratios with increasing molecular weight was observed for the L-CMP. However, the results indicate by and large a relatively uniform distribution of both radioisotopes throughout the molecular weight range of the multi-block copolymers.

In vitro metabolism studies of radiolabeled copolymers by Cathepsin S

In order to further investigate the metabolism of the multi-block copolymers, both ^{125}I- and ^{177}Lu-labeled S-CMP and L-CMP were incubated in the presence of Cat S. For the ^{125}I-labeled S-CMP and L-CMP, the degradation of the multi-block copolymers were analogous to the previous metabolism study. By the 1 h post-incubation time point, ^{125}I-S-CMP (Figure 4A) demonstrated a clear shift in retention to a single peak with a lower molecular weight. This new peak corresponds well to the elution volume of the monomeric block. Comparatively, at the 1 h time point, ^{125}I-labeled L-CMP (Figure 4B) exhibited a smaller shift to lower molecular weight and a much broader peak suggesting the presence of a mixture of products due to incomplete degradation. Additionally, the ^{125}I-labeled multi-block copolymers were incubated with human serum for 24 h. Both ^{125}I-labeled S-CMP and L-CMP demonstrated no signs of degradation by serum proteases.

The Cat S metabolism of the ^{177}Lu-labeled S-CMP and L-CMP demonstrated a significant contrast relative to the ^{125}I-labeled, multi-block copolymers. For ^{177}Lu-labeled S-CMP (Figure 4C), the degradation of the multi-block copolymer by 1 h revealed two peaks at 7.3 and 9.3 mL. Based on the elution volumes, these peaks correspond, respectively, to ^{177}Lu

bound to the monomeric blocks (61.4 % Area Under the Curve (AUC)) and ^{177}Lu associated with the released peptide fragment (38.6 % AUC). By 24 h post-incubation, the percentage of signal corresponding to the small molecule fragment increased (51.1 % AUC), but the release of the ^{177}Lu from the monomeric blocks remained incomplete. Similar, but slower degradation profiles were observed for ^{177}Lu-labeled L-CMP. At 1 h after incubation with Cat S, the GPC profile of ^{177}Lu-labeled S-CMP (Figure 4D) showed that only 12.6 % of the signal corresponded to the small peptide fragment. By 24 h, the AUC for the small molecule fragments had increased to 41.1 %.

Cell uptake, trafficking and cleavage studies

Confocal microscopy was used to examine the *in vitro* uptake and cell trafficking profiles of the multi-block copolymers by hMDM and HPAC human pancreatic ductal adenocarcinoma cells. To that end, S-CMP and L-CMP, which contains conjugated Cy5, were incubated with both cells lines for 12 h and counterstained with Lysotracker® Red and DAPI to identify the endolysosomal compartments and the nucleus, respectively. The confocal images of the hMDM (Figure 5A) and HPAC cells (Figure S7) were examined and the mean fluorescence was quantified (Figure 5B). The mean fluorescence measurements showed that the hMDM uptake of S-CMP and L-CMP was 17.5 and 23.8 times higher, correspondingly, compared to HPAC cells. No statistical differences in uptake were observed between S-CMP and L-CMP in the same cell type. For the hMDM, the internalized Cy5 signals strongly corresponded to the acidic compartments denoted by the Lysotracker® Red signal, with correlations of 0.89 $\pm$ 0.02 (n = 9) and 0.92 $\pm$ 0.02 (n = 9) for S-CMP and L-CMP, respectively. This indicates that the internalized multi-block copolymers reside in the endolysosomal compartments of the hMDM, which are known to exhibit one of the highest intracellular activities of Cat S.[23]

To evaluate the cleavage rate of the multi-block copolymers by hMDM, ^{125}I-labeled S-CMP and L-CMP were individually incubated with hMDM and used differentiation medium, results are shown in Figure S6. Similar to the Cat S cleavage studies depicted in Figure 4A and 4B, the ^{125}I-labeled S-CMP was efficiently cleaved by hMDM after 12 h of incubation, while a substantially lower rate of L-CMP cleavage was observed under the same conditions. Incubation of the multi-block copolymers with used media, obtained from hMDM culture, found no evidence of degradation. This strongly suggests that the cleavage of the copolymers was due to the uptake and processing by the hMDM.

Biodistribution and metabolism studies of dual-labeled copolymers

Dual-isotope biodistribution studies were performed with the intended purpose of shedding light on the *in vivo* degradation kinetics of the multi-block copolymers. Due to the lower photon abundance and shorter half-life of ^{177}Lu relative ^{125}I, ^{125}I- and ^{177}Lu-labeled S-CMPs and L-CMPs were administered to HPAC xenograft bearing SCID mice at a 1:3 radioisotopic ratio, correspondingly. The tissue biodistribution profiles of the copolymer block, represented by the ^{125}I signal, and the Cat S-susceptible peptide, represented by the ^{177}Lu signal, are displayed in Figure 6 and Figure 7 (the corresponding values were shown in Table S2 and S3), respectively. Our expectation was that the multi-block copolymers will fragment over time leading to the generation and clearance of both the ^{177}Lu-labeled peptide fragment and the ^{125}I-monomeric blocks from non-target tissues.

We also anticipated that the generated peptide fragments would clear relatively quickly after generation compared to the larger copolymeric blocks, allowing us to use $^{125}I/^{177}Lu$ ratios as a measure of the relative speed of the *in vivo* degradation and clearance of the multi-block copolymers.

For the ^{125}I-labeled multi-block copolymers, the excretion profiles of the S-CMP at late time points (72 and 144 h) were significantly higher ($p < 0.05$) relative to the L-CMP. By the 144 h time point, 60.07 ± 1.95 %ID of the ^{125}I-labeled S-CMP had cleared from the mouse compared to 40.42 ± 1.89 %ID of the ^{125}I-labeled L-CMP. Interestingly, at early time points, the pattern had been reversed with L-CMP demonstrating higher excretion. Additionally, the $^{125}I/^{177}Lu$ ratio for the urine at 4 h counterintuitively suggests that ^{125}I (copolymer block) was being excreted faster than the ^{177}Lu (small peptide fragment). Since the multi-block copolymers are primarily excreted through the kidneys, these findings prompted us to perform GPC-HPLC analysis of the urine, depicted in Figure 8, for both ^{125}I-labeled S-CMP and L-CMP. The results showed that the majority (63.3 % for S-CMP and 57.7 % for L-CMP) of the radio-signal in urine from first 4 h corresponded to a low molecular weight ^{125}I molecule(s). This implies that deiodination of the ^{125}I-labeled Tyr-MA of the copolymers is occurring *in vivo* leading to higher than expected renal clearance of the ^{125}I from the mice. However, relatively small amounts of deiodination products were observed in the urine during the time period of 4 – 72 h (16.9 % for S-CMP and 12.5 % for L-CMP) and 72– 144 h (less than 5 % for both copolymer). In addition, biodistribution of these animals at 144h p.i. revealed that the thyroid uptake (Table S4) of the multi-block copolymers, known to be high for unstable radioiodinated compounds, was similar or lower than muscle. In all, these studies demonstrate that the in vivo deiodination was largely limited to the early 4h time-point and should have no significant effect on the interpretation of the biodistribution results.

The blood retention of the S-CMP was significantly lower ($p < 0.05$) than the L-CMP at all time points investigated. The relative differences in blood retention between the two ^{125}I-labeled multi-block copolymers increased with time, yielding a maximum differential at 144 h p.i. with 1.22 ± 0.82 %ID/g for S-CMP and 3.92 ± 0.71 %ID/g for L-CMP. For the L-CMP, the $^{125}I/^{177}Lu$ ratios for the blood, tabulated in Table 4, are relatively constant at all times. However, notably, the $^{125}I/^{177}Lu$ ratios for S-CMP are reduced by half. A hallmark of MPS-associated uptake is the accumulation of polymeric drug delivery systems in the liver and spleen. Our approach of utilizing Cat S-susceptible linkers seeks to reduce this non-target MPS accumulation. Based on the ^{125}I-labeled multi-block copolymer profiles, the S-CMP demonstrated significantly lower accumulation in the liver and spleen compared to the L-CMP. As was seen in the blood, the divergent retention of the two multi-block copolymers in both of these tissues grew longitudinally. By 144 p.i., the liver and spleen retention of the S-CMP was 3.31 and 4.95 fold lower that the L-CMP, respectively. For both of the multi-block copolymers, the liver and spleen $^{125}I/^{177}Lu$ ratios demonstrated no significant changes over the initial 24 h time period. By 72 h, significant increases in the ratios were seen for both copolymer systems in both tissues. At 144 h, the liver had the highest $^{125}I/^{177}Lu$ ratios, 1.32 ± 0.12 for S-CMP and 1.53 ± 0.06 for L-CMP, of any tissue investigated, suggesting degradation and clearance of the multi-block copolymers is particularly efficient in the liver. The highest spleen $^{125}I/^{177}Lu$ ratios were also observed at 144 h, but these ratios were on average lower than analogous liver values.

Unlike the uptake and retention profiles for the blood, liver and spleen, no significant differences in HPAC tumor accumulation was observed for the two multi-block copolymers. This suggests that differences in the molecular size of the multi-block copolymers had no measureable effect on the EPR effect based deposition. The highest level of HPAC tumor accumulation for ^{125}I-labeled multi-block copolymers were observed at 72 h with 13.87 ± 2.74 %ID/g for S-CMP and 12.45 ± 1.95 %ID/g for L-CMP. By 144 h, these values correspondingly declined to 9.65 ± 1.10 %ID/g and 9.43 ± 1.95 %ID/g. At 72 and 144 h time points, the substantial tumor accumulation and enhanced non-target clearance resulted in tumor to non-target ratios, tabulated in Table S5, that were substantially higher than unity for most tissues, particularly for the S-CMP. Interestingly, the ^{125}I/^{177}Lu ratios for the HPAC tumors increased from 0.57 ± 0.11 and 0.87 ± 0.08 at 4 h to 0.99 ± 0.09 and 1.13 ± 0.05 by 144 h for S-CMP and L-CMP, respectively. This implies that over time the multi-block copolymers are degraded in the HPAC tumors. Although, importantly, this does not lead to as significant of a reduction in tumor retention of the copolymeric blocks as it does for MPS-associated tissues.

DISCUSSION

The utilization of peptide cleavable linkers has long been employed in the field of drug delivery, primarily as a means of drug release from the delivery platform.[24] For chemotherapeutic formulations with HPMA copolymers, Kopecek and others have utilized cathepsin B-susceptible peptide linkers not only for drug release, but to also improve the biodegradability and excretion of the HPMA copolymer.[25–28] Since cathepsin B is ubiquitously expressed, the degradation rate of the copolymer and release of the conjugated chemotherapeutics would be expected to occur relatively uniformly for the most part in any tissue taking up the polymer conjugate. Our laboratory is focused on the utilization of Cat S-cleavable peptide linkers to increase the translational potential of radiopharmaceuticals. Cat S is a protease that is selectively and highly expressed in the phagocytic cells of the MPS and therefore in MPS-associated tissues (e.g., blood, liver and spleen). The MPS is also known to be a large contributor to the sequestration of drug delivery platforms.[29] By developing Cat S-cleavable linkers, we seek to selectively exploit the higher levels of cathepsin S expression in MPS-associated, non-target tissues relative to the levels expressed in many tumors[16, 30]. The goal of this approach is to increase the clearance of the radiolabeled agent from MPS-associated non-target tissues, due to more rapid degradation, relative to tumors thus achieving improvements in the T/NT ratios. Indeed, using HPMA copolymer, our early work demonstrated that incorporation of a cathepsin S-cleavable linker led to significant improvement in T/NT ratios compared to a known cathepsin B-cleavable linker.[15]

Our laboratory has explored the incorporation of Cat S-susceptible linkers into the side chain or backbone of HPMA copolymers to investigate how these structural modifications impact biological performance.[16, 17] However, to date, the impact of the copolymer block size on the cleavage and biodistribution profile of Cat-S-cleavable, mutli-block HPMA copolymers has not been studied. The molecular weight of copolymers and the degraded fragments is expected to play a key factor affecting the biological performance of the diagnostic agent. In order to evaluate the block size influence on the *in vitro* and *in vivo* behavior of Cat S-

susceptible HPMA copolymers and monitor the cleavage rates of these agents in different organs, we synthesized two multi-block HPMA copolymers, S-CMP (92.5 kDa) and L-CMP (145 kDa), extended from HPMA copolymer blocks of 17.4 and 32.9 kDa, respectively. The Cat S-cleavable, HPMA copolymers were dual-labeled using [177]Lu (peptide linker) and [125]I (copolymer block). The biological performance of these two Cat S-susceptible, multi-block HPMA copolymers were investigated.

Cat S cleavage studies of the S-CMP and L-CMP revealed that the molecular weight of the copolymers has a remarkable impact on the degradation rate. Fragmentation of the S-CMP appeared to be essentially complete by 1 h incubation with Cat S relative to only 30% for the L-CMP. This observation is almost certainly a result of the larger steric hindrance to the protease due to the increased polymeric size of the L-CMP. Similarly, this trend was also observed for the Cat S cleavage studies of the ^{125}I-labeled, multi-block copolymers. Interestingly, the ^{177}Lu-labeled, multi-block copolymer demonstrated fragmentation into lower molecular weight polymeric units, but did not completely convert into the expected small molecular weight peptide fragments. As shown in Figure 4C and 4D, 48.9 and 58.9 % of the ^{177}Lu signal for the S-CMP and L-CMP, correspondingly, was associated with the fragmented polymeric blocks after 24 h of incubation with Cat S. This suggests that the first cleavage of the Cat S-susceptible copolymers is relatively fast, but the second cleavage, that generates the low molecular weight fragment, is significantly slower. We postulate that the incomplete fragmentation of the peptide is due to increased association of the attached peptide fragment with the polymeric backbone after the first cleavage by Cat S takes place.

Phagocytic cells, such as monocytes and macrophages, constitute the MPS[31] and are major contributors to the *in vivo* sequestration of nanomedicine platforms.[32] It is well known that monocytes and macrophages express high intracellular levels of Cat S due to their role in antigen presentation.[33] Confocal microscopy studies showed that S-CMP and L-CMP were much more actively taken up by hMDM in comparison to the HPAC cells. However, no statistical differences in uptake were observed between the two multi-block copolymers when comparing the same cell type, suggesting that the size differential utilized in this study did not play a major factor in influencing the uptake and retention of these agents. Internalization of both multi-block HPMA copolymers led to accumulation in the endolysosomal compartments, which contain the highest cellular concentration of Cat S.[23] Using the Förster Resonance Energy Transfer (FRET) technique, we have previously demonstrated that the utilized Cat S-cleavable peptide, P-M-G-L-P, can be efficiently cleaved in the endolysosomal compartments of hMDM and are eventually effluxed.[17] Incubation of S-CMP and L-CMP with hMDM confirmed that the S-CMP was degraded more rapidly by hMDM compared to the L-CMP. These results correlated well with the previous cleavage studies using Cat S. Many human tumor types are known to have a substantial macrophage composition.[34] Indeed, tumor-associated macrophages (TAMs) have been shown to sequester substantially higher concentrations of nanomedicine platforms relative to tumor cells.[35, 36] Extrapolating these finding to our *in vivo* results suggests that tumor-associated macrophages may be a major contributor to the observed *in vivo* degradation of the multi-block HPMA copolymers in the tumor.

For the *in vivo* investigations, a dual-isotope labeling approach was utilized for the multi-block copolymers. This methodology, which has been employed by others groups,[37, 38] offers a convenient way to simultaneously measure the biodistribution of multi-component systems. In this instance, instead of the simultaneous labeling of the copolymer, we prepared ^{125}I-labeled and ^{177}Lu-labeled copolymers separately and formulated the desired radioisotope ratios before administration. Two advantages could be achieved by this strategy: 1) the separate labeling allowed for easy and precise quantification of the single-labeled copolymer and 2) the radioisotope ratios in the formulation could be readily altered as needed for studies. One potential concern with any dual-isotope labeled agent is whether the isotopes are homogenously distributed in the carrier. Fractionation of the dual-isotope formulation revealed no significant differences in the distribution of the two radioisotopes throughout the molecular weight range of the multi-block HPMA copolymer. Importantly, this signifies that the dual-isotope labeled, multi-block HPMA copolymer would give a true account of the disposition of the polydisperse carrier *in vivo*.

Our laboratory has previously demonstrated that multi-block copolymers fragment and clear from the non-target tissues and the body more effectively than analogous non-degradable copolymers.[17] It was anticipated that the peptide fragment, labeled with ^{177}Lu, would clear more quickly than the fragmented polymeric blocks, labeled with ^{125}I, due to substantially lower molecular weight. However, to our surprise, ^{125}I was cleared from the mice more quickly than ^{177}Lu at early time points (4 and 24 h). This prompted us to study the excretion using just the ^{125}I-labeled S-CMP and L-CMP and examine the radio-GPC profile of the urine. These studies revealed that in the first 4 h the majority of the ^{125}I signal corresponded to small molecules, which indicates that some deiodination of the copolymer occurs *in vivo*. Though, the percentage of deiodination products in the urine quickly decreased at subsequent time points. This observation is not too surprising given that the *in vivo* deiodination of radioiodinated carriers is well established.[39, 40] The thyroid is a known scavenger of free iodide[41] and significant uptake in this tissue is a strong indicator of in vivo deiodination. Analysis of the thyroid uptake at 144 h demonstrated low levels, similar to muscle, of iodide uptake. Taken together, this establishes that the observed deiodination does not have a substantive impact on the interpretation of the biodistribution studies.

Lower blood retention was observed for S-CMP relative to L-CMP, likely due to the faster cleavage kinetics of the smaller copolymer size. Since both multi-block copolymers were shown to be stable in serum stability studies, it is presumed that some degradation in the blood occurs through uptake and processing by resident phagocytic cells, such as monocytes. Interestingly, the ^{125}I/^{177}Lu ratios for the S-CMP decreased over time while the ratios for the L-CMP remained essentially constant. The significant decrease in ^{125}I/^{177}Lu ratios for S-CMP is almost certainly associated with the faster cleavage and clearance kinetics of the S-CMP fragments. We speculate this observation is due to two factors: 1) the faster renal clearance of the ^{125}I-labeled copolymer fragments of the S-CMP from circulation and 2) increased blood concentration of the ^{177}Lu peptide fragments due to the reabsorption of the peptide fragment from solid tissues.

The uptake of drug delivery systems in the liver, spleen and other MPS-associated tissues is largely due to the uptake by tissue-resident macrophages (e.g., Kupffer cells) and the

fenestrated vasculature endothelium in some tissues.[42] For the liver and spleen, initial uptake of the multi-block HPMA copolymers were identical, but retention of the two constructs started to diverge by 24 h post-administration. Substantially higher levels of liver and spleen clearance were seen for both the copolymer and peptide fragments for the S-CMP relative to the L-CMP, which we attribute to the faster cleavage and clearance kinetics of the S-CMP. For both multi-block HPMA copolymers, significant changes ($p < 0.01$) to the $^{125}I/^{177}Lu$ ratios for the liver and spleen were not observed until 72 h. This suggests the majority of the processing (i.e., fragmentation and clearance) of these multi-block copolymers in these tissues does not occur during the first 24 h, but begins after this time point and continues through the time points investigated.

Both of the multi-block copolymers demonstrated a substantial level of uptake in HPAC tumor, through the EPR effect, with no statistically significant difference between the two constructs. In the tumor, as with the liver and spleen, the $^{125}I/^{177}Lu$ ratios for both multi-block HPMA copolymers increased over time, indicating that cleavage of the multi-block copolymers does indeed occur in the tumor. Based on the *in vitro* confocal studies, the hMDM are much more apt to take-up/internalize the copolymers relative to the HPAC cells. Additionally, as stated before, TAMs are known to constitute a significant portion of the mass of many tumors and sequester significant concentrations of nanomedicine platforms.[35, 36, 43] Given all this information, we postulate that the majority of the degradation observed in the tumor is due to phagocytic immune cells such as TAMs. While the data clearly shows that the multi-block HPMA copolymers are degraded in the tumor, albeit at a slower rate than the liver, it is important to recognize that this degradation does not impact the retention of the copolymer fragments in the tumor as much as it does in non-target tissues. This is probably owing to the lack of effective lymphatic drainage from the HPAC tumors,[44] which is part of the EPR effect, diminishing the amount of fragmented copolymer that is able to clear the tumor upon degradation. This phenomenon is certainly favorable to diagnostic imaging as it promotes the generation of higher T/NT ratios.

CONCLUSION

In this study, we investigated the effect of copolymeric block size on the *in vitro* and *in vivo* properties of Cat S-susceptible, HPMA copolymers. To that end, two multi-block copolymers, S-CMP and L-CMP, were developed, in which the copolymer blocks and the peptidic linkers were tagged with ^{125}I and ^{177}Lu, respectively. The *in vitro* studies showed that S-CMP, the smaller block size construct, had increased Cat S cleavage rates likely due to less steric hindrance. Block size did not impact the uptake and retention of the two multi-block copolymers in hMDM or HPAC pancreatic ductal adenocarcinoma cells. The S-CMP demonstrated significantly faster clearance from non-targeted tissue relative to L-CMP. Mechanistically, the multi-block copolymers show different tissue-dependent rates with regard to fragmentation and clearance, with the liver showing the highest levels. Notably, the tumor retention of the fragmented copolymers was significantly higher than non-target retention leading to the generation of favorable T/NT ratios. Overall, the results demonstrate that the block size plays an important role in the biological performance of Cat S-degradable polymeric constructs.

Supplementary Material

Refer to Web version on PubMed Central for supplementary material.

Acknowledgments

References

1. Fass L. Imaging and cancer: a review. Mol Oncol. 2008; 2:115–152. [PubMed: 19383333]

2. Tummala P, Junaidi O, Agarwal B. Imaging of pancreatic cancer: An overview. J Gastrointest Oncol. 2011; 2:168–74. [PubMed: 22811847]

3. Bouchelouche K, Oehr P. Positron emission tomography and positron emission tomography/computerized tomography of urological malignancies: an update review. J Urol. 2008; 179:34–45. [PubMed: 17997425]

4. Reshef A, Shirvan A, Akselrod-Ballin A, Wall A, Ziv I. Small-molecule biomarkers for clinical PET imaging of apoptosis. J Nucl Med. 2010; 51:837–840. [PubMed: 20484422]

5. Agdeppa ED, Spilker ME. A review of imaging agent development. AAPS J. 2009; 11:286–299. [PubMed: 19415506]

6. England CG, Hernandez R, Eddine SBZ, Cai W. Molecular imaging of pancreatic cancer with antibodies. Mol Pharm. 2015; 13:8–24. [PubMed: 26620581]

7. Lammers T, Aime S, Hennink WE, Storm G, Kiessling F. Theranostic nanomedicine. Acc Chem Res. 2011; 44:1029–38. [PubMed: 21545096]

8. Raha S, Paunesku T, Woloschak G. Peptide-mediated cancer targeting of nanoconjugates. Wiley Interdiscip Rev Nanomed Nanobiotechnol. 2011; 3:269–81. [PubMed: 21046660]

9. Song G, S Petschauer J, J Madden A, C Zamboni W. Nanoparticles and the mononuclear phagocyte system: pharmacokinetics and applications for inflammatory diseases. Curr Rheumatol Rev. 2014; 10:22–34. [PubMed: 25229496]

10. Kope ek J, Kope ková P. HPMA copolymers: origins, early developments, present, and future. Adv Drug Deliv Rev. 2010; 62:122–149. [PubMed: 19919846]

11. Pike DB, Ghandehari H. HPMA copolymer-cyclic RGD conjugates for tumor targeting. Adv Drug Deliv Rev. 2010; 62:167–183. [PubMed: 19951733]

12. Lu Z-R. Molecular imaging of HPMA copolymers: visualizing drug delivery in cell, mouse and man. Adv Drug Deliv Rev. 2010; 62:246–257. [PubMed: 20060431]

13. Hoffmann S, Vystr ilová L, Ulbrich K, Etrych T, Caysa H, Mueller T, Mäder K. Dual fluorescent HPMA copolymers for passive tumor targeting with pH-sensitive drug release: synthesis and characterization of distribution and tumor accumulation in mice by noninvasive multispectral optical imaging. Biomacromolecules. 2012; 13:652–663. [PubMed: 22263698]

14. Zarabi B, Borgman MP, Zhuo J, Gullapalli R, Ghandehari H. Noninvasive monitoring of HPMA copolymer-RGDfK conjugates by magnetic resonance imaging. Pharm Res. 2009; 26:1121–1129. [PubMed: 19160028]

15. Ogbomo SM, Shi W, Wagh NK, Zhou Z, Brusnahan SK, Garrison JC. ^{177}Lu-labeled HPMA copolymers utilizing cathepsin B and S cleavable linkers: synthesis, characterization and preliminary in vivo investigation in a pancreatic cancer model. Nucl Med Biol. 2013; 40:606–617. [PubMed: 23622691]

16. Shi W, Ogbomo SM, Wagh NK, Zhou Z, Jia Y, Brusnahan SK, Garrison JC. The influence of linker length on the properties of cathepsin S cleavable ^{177}Lu-labeled HPMA copolymers for pancreatic cancer imaging. Biomaterials. 2014; 35:5760–5770. [PubMed: 24755528]

17. Fan W, Shi W, Zhang W, Jia Y, Zhou Z, Brusnahan SK, Garrison JC. Cathepsin S-cleavable, multi-block HPMA copolymers for improved SPECT/CT imaging of pancreatic cancer. Biomaterials. 2016; 103:101–15. [PubMed: 27372424]

18. Duncan R, Cable H, Rejmanová P, Kope ek J, Lloyd J. Tyrosinamide residues enhance pinocytic capture of N-(2-hydroxypropyl) methacrylamide copolymers. Biochim Biophys Acta, Gen Subj. 1984; 799:1–8.

19. Li C, Winnard PT, Takagi T, Artemov D, Bhujwalla ZM. Multimodal image-guided enzyme/prodrug cancer therapy. J Am Chem Soc. 2006; 128:15072–15073. [PubMed: 17117842]

20. Lützner N, Kalbacher H. Quantifying cathepsin S activity in antigen presenting cells using a novel specific substrate. J Biol Chem. 2008; 283:36185–36194. [PubMed: 18957408]

21. Dunford HB, Ralston IM. On the mechanism of iodination of tyrosine. Biochem Biophys Res Commun. 1983; 116:639–643. [PubMed: 6651828]

22. Schwarz G, Mueller L, Beck S, Linscheid MW. DOTA based metal labels for protein quantification: a review. J Anal At Spectrom. 2014; 29:221–233.

23. Kirschke H, Wiederanders B. Cathepsin S and related lysosomal endopeptidases. Methods Enzymol. 1994; 244:500–511. [PubMed: 7845228]

24. Hu Q, Katti PS, Gu Z. Enzyme-responsive nanomaterials for controlled drug delivery. Nanoscale. 2014; 6:12273–12286. [PubMed: 25251024]

25. Larson N, Yang J, Ray A, Cheney DL, Ghandehari H, Kope ek J. Biodegradable multiblock poly(N-2-hydroxypropyl) methacrylamide gemcitabine and paclitaxel conjugates for ovarian cancer cell combination treatment. Int J Pharm. 2013; 454:435–443. [PubMed: 23827653]

26. Mužíková G, Pola R, Laga R, Pechar M. Biodegradable Multiblock Polymers Based on N-(2-Hydroxypropyl) methacrylamide Designed as Drug Carriers for Tumor-Targeted Delivery. Macromol Chem Phys. 2016; 217:1690–1703.

27. Zhang R, Luo K, Yang J, Sima M, Sun Y, Janát-Amsbury MM, Kope ek J. Synthesis and evaluation of a backbone biodegradable multiblock HPMA copolymer nanocarrier for the systemic delivery of paclitaxel. J Control Release. 2013; 166:66–74. [PubMed: 23262201]

28. Pan H, Sima M, Miller SC, Kope ková P, Yang J, Kope ek J. Efficiency of high molecular weight backbone degradable HPMA copolymer–Prostaglandin E 1 conjugate in promotion of bone formation in ovariectomized rats. Biomaterials. 2013; 34:6528–6538. [PubMed: 23731780]

29. Blanco E, Shen H, Ferrari M. Principles of nanoparticle design for overcoming biological barriers to drug delivery. Nat Biotechnol. 2015; 33:941–951. [PubMed: 26348965]

30. von Burstin J, Eser S, Seidler B, Meining A, Bajbouj M, Mages J, Lang R, Kind AJ, Schnieke AE, Schmid RM. Highly sensitive detection of early-stage pancreatic cancer by multimodal near-infrared molecular imaging in living mice. Int J Cancer. 2008; 123:2138–2147. [PubMed: 18709639]

31. Chow A, Brown BD, Merad M. Studying the mononuclear phagocyte system in the molecular age. Nat Rev Immunol. 2011; 11:788–798. [PubMed: 22025056]

32. Moghimi SM, Hunter AC, Murray JC. Nanomedicine: current status and future prospects. FASEB J. 2005; 19:311–330. [PubMed: 15746175]

33. Petanceska S, Canoll P, Devi LA. Expression of rat cathepsin S in phagocytic cells. J Biol Chem. 1996; 271:4403–4409. [PubMed: 8626791]

34. Mantovani A, Schioppa T, Porta C, Allavena P, Sica A. Role of tumor-associated macrophages in tumor progression and invasion. Cancer Metastasis Rev. 2006; 25:315–322. [PubMed: 16967326]

35. Miller MA, Zheng Y, Gadde S, Pfirschke C, Zope H, Engblom C, Kohler RH, Iwamoto Y, Yang KS, Askevold B, Kolishetti N, Pittet M, Lippard SJ, Farokhzad OC, Weissleder R. Tumour-associated macrophages act as a slow-release reservoir of nano-therapeutic Pt(IV) pro-drug. Nat Commun. 2015; 6:8692. [PubMed: 26503691]

36. Vinogradov S, Warren G, Wei X. Macrophages associated with tumors as potential targets and therapeutic intermediates. Nanomedicine. 2014; 9:695–707. [PubMed: 24827844]

37. Hijnen NM, Vries A, Nicolay K, Grüll H. Dual-isotope ^{111}In/^{177}Lu SPECT imaging as a tool in molecular imaging tracer design. Contrast Media Mol Imaging. 2012; 7:214–222. [PubMed: 22434634]

38. Zhang R, Yang J, Sima M, Zhou Y, Kope ek J. Sequential combination therapy of ovarian cancer with degradable N-(2-hydroxypropyl) methacrylamide copolymer paclitaxel and gemcitabine conjugates. Proc Natl Acad Sci U S A. 2014; 111:12181–12186. [PubMed: 25092316]

39. BakkerWH KE, Breenian W. Receptorscintigraphy with a radioiodinated somatostatin analogue: radiolabeing, purification, biolo gic activity, and in vivo application in animals. J Nucl Med. 1990; 31:1501–1509. [PubMed: 1975618]

40. Sinsheimer J, Wang T, Röder S, Shum Y. Mechanisms for the biodehalogenation of iodocompounds. Biochem Biophys Res Commun. 1978; 83:281–286. [PubMed: 697816]

41. Leung A, Pearce EN, Braverman LE. Role of iodine in thyroid physiology. Expert Rev Endocrinol Metab. 2010; 5:593–602.

42. van Hinsbergh VW. Endothelial permeability for macromolecules Mechanistic aspects of pathophysiological modulation. Arterioscler Thromb Vasc Biol. 1997; 17:1018–1023. [PubMed: 9194749]

43. Sica A, Schioppa T, Mantovani A, Allavena P. Tumour-associated macrophages are a distinct M2 polarised population promoting tumour progression: potential targets of anti-cancer therapy. Eur J Cancer. 2006; 42:717–727. [PubMed: 16520032]

44. Olszewski WL, Stanczyk M, Gewartowska M, Domaszewska-Szostek A, Durlik M. Lack of functioning intratumoral lymphatics in colon and pancreas cancer tissue. Lymphat Res Biol. 2012; 10:112–117. [PubMed: 22984907]
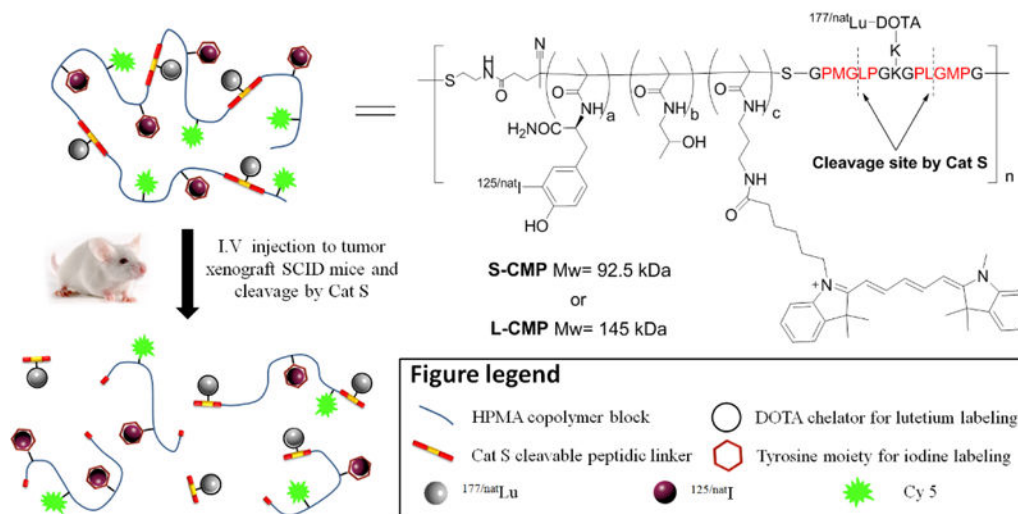
Figure 1.
Schematic design, cleavage, and clearance of the duo-labeled cathepsin S-susceptible, multi-block HPMA copolymers.
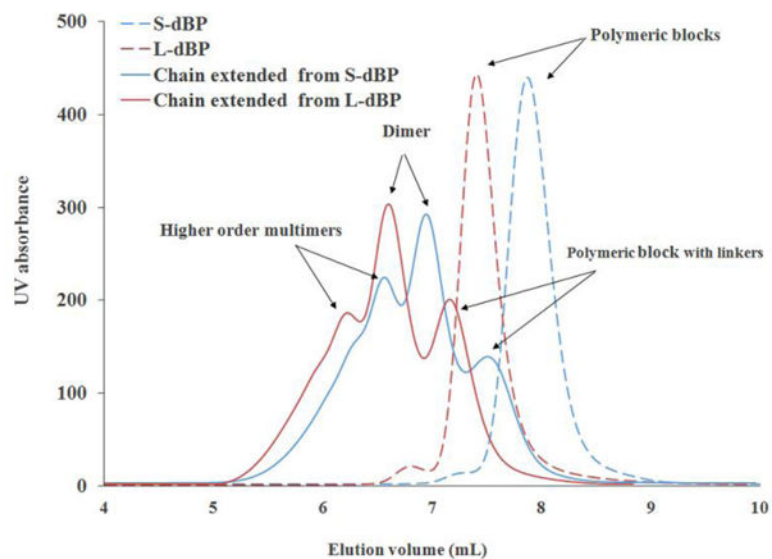
Figure 2.
GPC profile of deprotected HPMA telechelic block copolymer (S-dMP or L-dMP) before and after chain extension by Cat S susceptible linker.
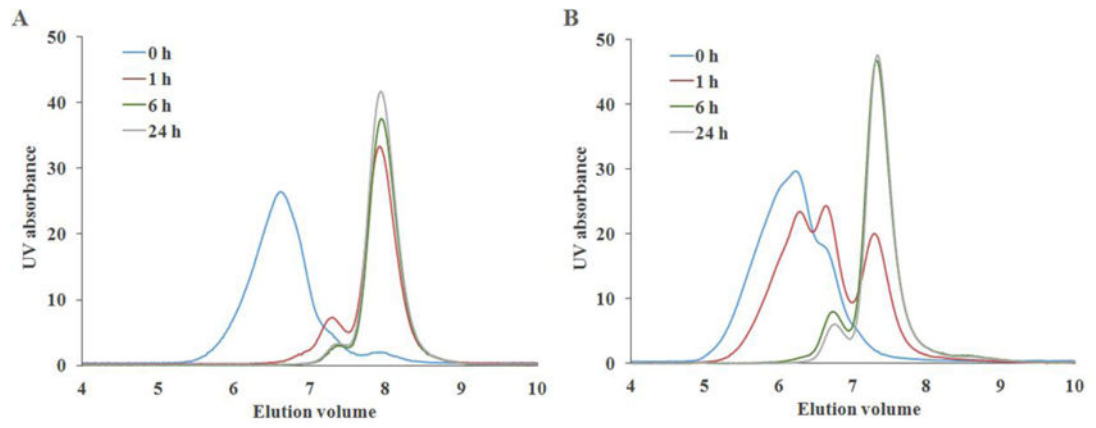
Figure 3.
GPC profile of multi-block HPMA copolymers (S-CMP (**A**) or L-CMP (**B**)) and degradation products after incubation with Cat S at different time intervals.
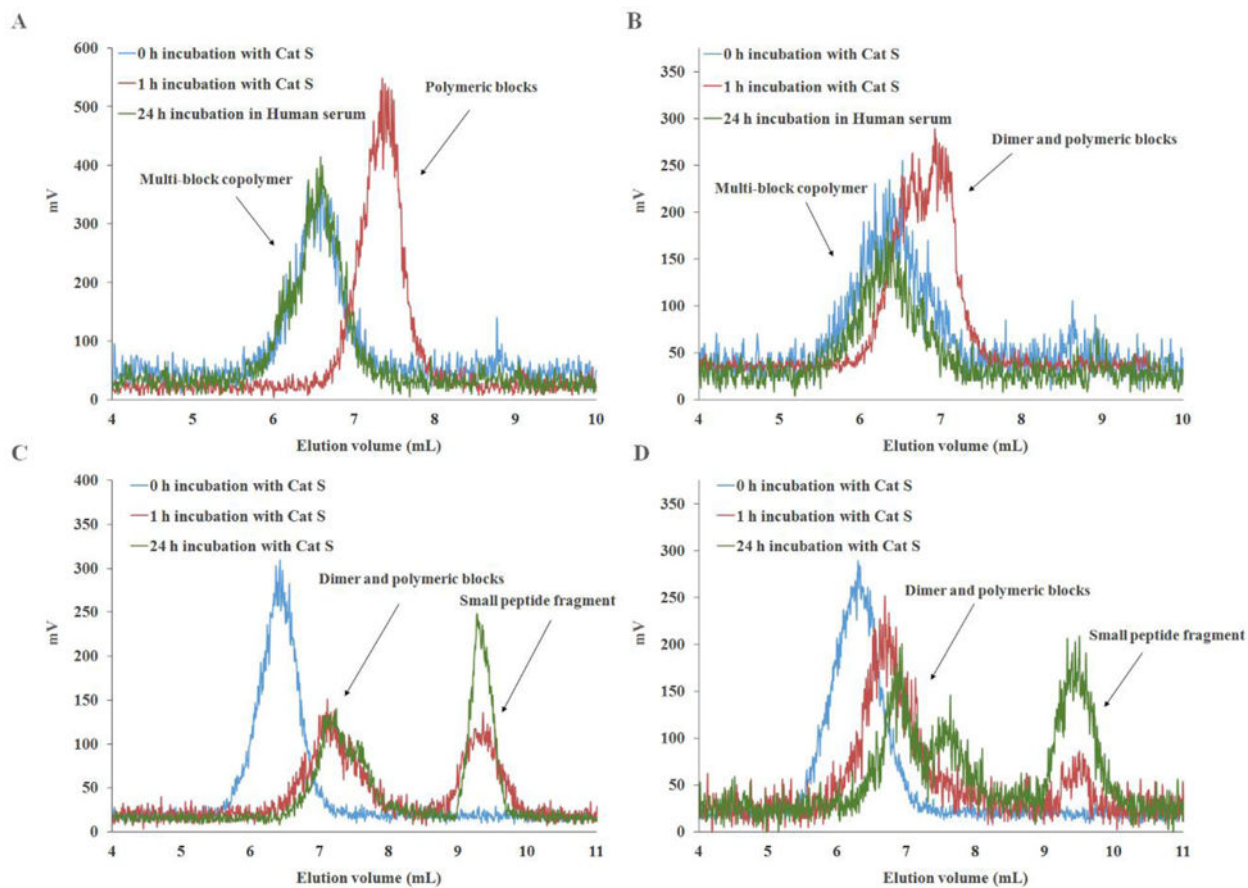
Figure 4.
Radio-GPC profiles of ^{125}I-S-CMP (**A**) and ^{125}I-L-CMP (**B**), correspondingly, before and after incubation with Cat S for 1 h and exposure to human plasma for 24 h. The cleavage studies of ^{177}Lu-S-CMP (**C**) and ^{177}Lu-L-CMP (**D**) by Cat S at 0, 1 and 24 h.
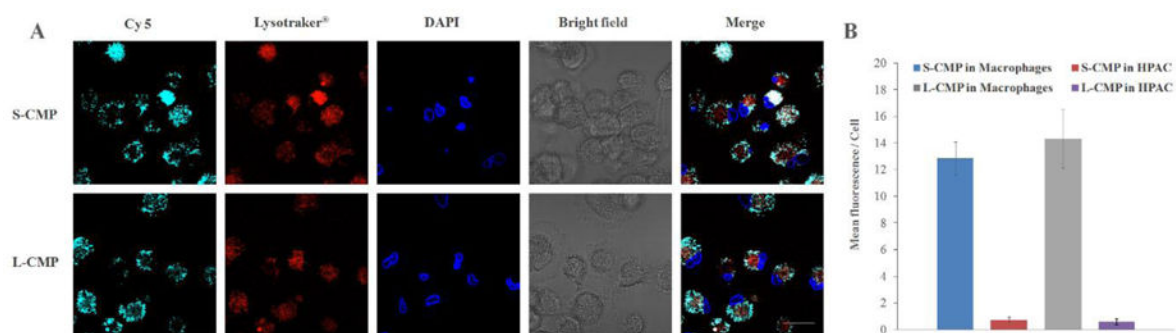
Figure 5.
Representative confocal microscopy images of macrophages incubated with S-CMP and L-CMP at 12 h (**A**), respectively. Lysotracker (red) visualized endolysosomal compartments, DAPI (blue) denotes the nucleus and Cy 5 (cyan) is associated with the copolymer. Scale bar = 20 μm. The mean florescent intensities of Cy5 per cell in macrophages and HPAC cells (**B**).
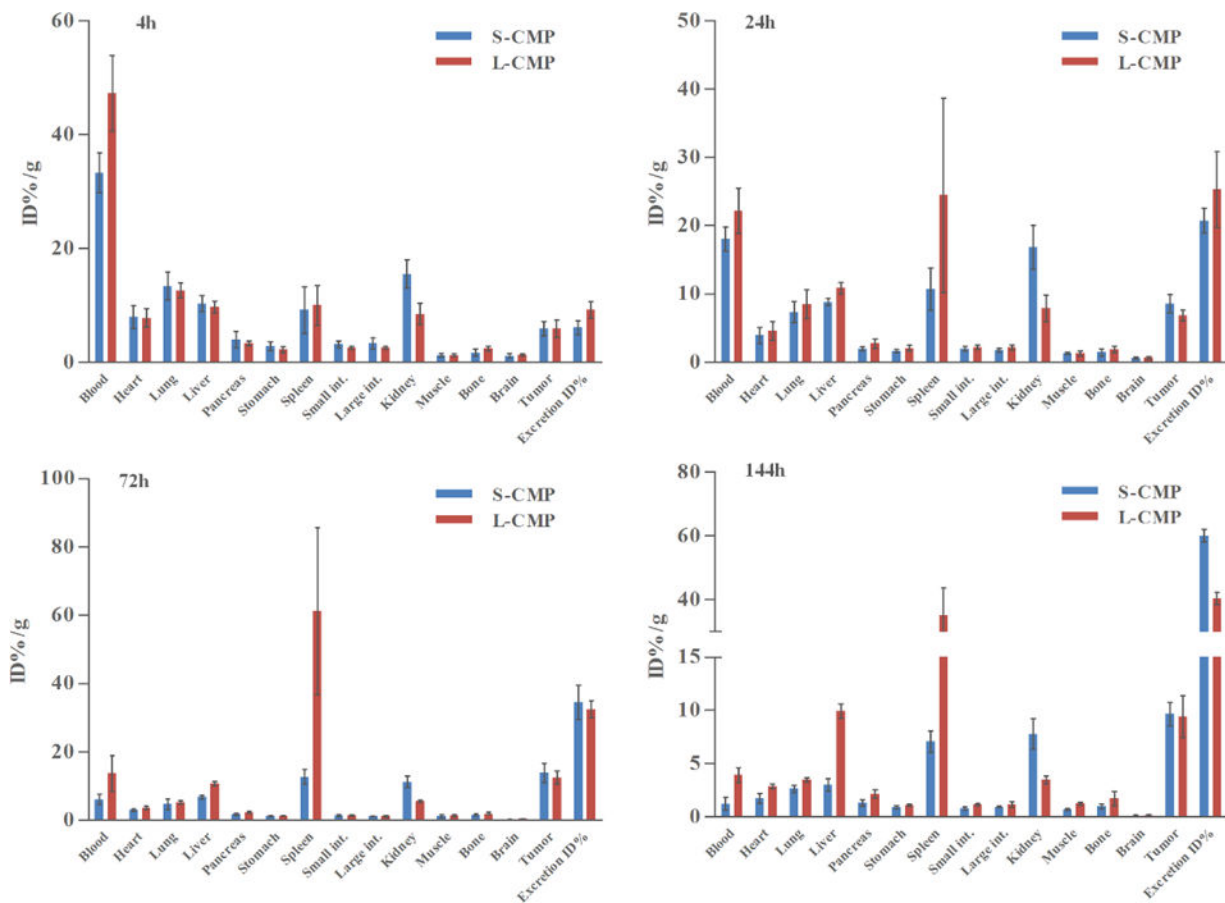
Figure 6.
Biodistribution data of ^{125}I-labeled copolymers in a HPAC tumor bearing mouse model.
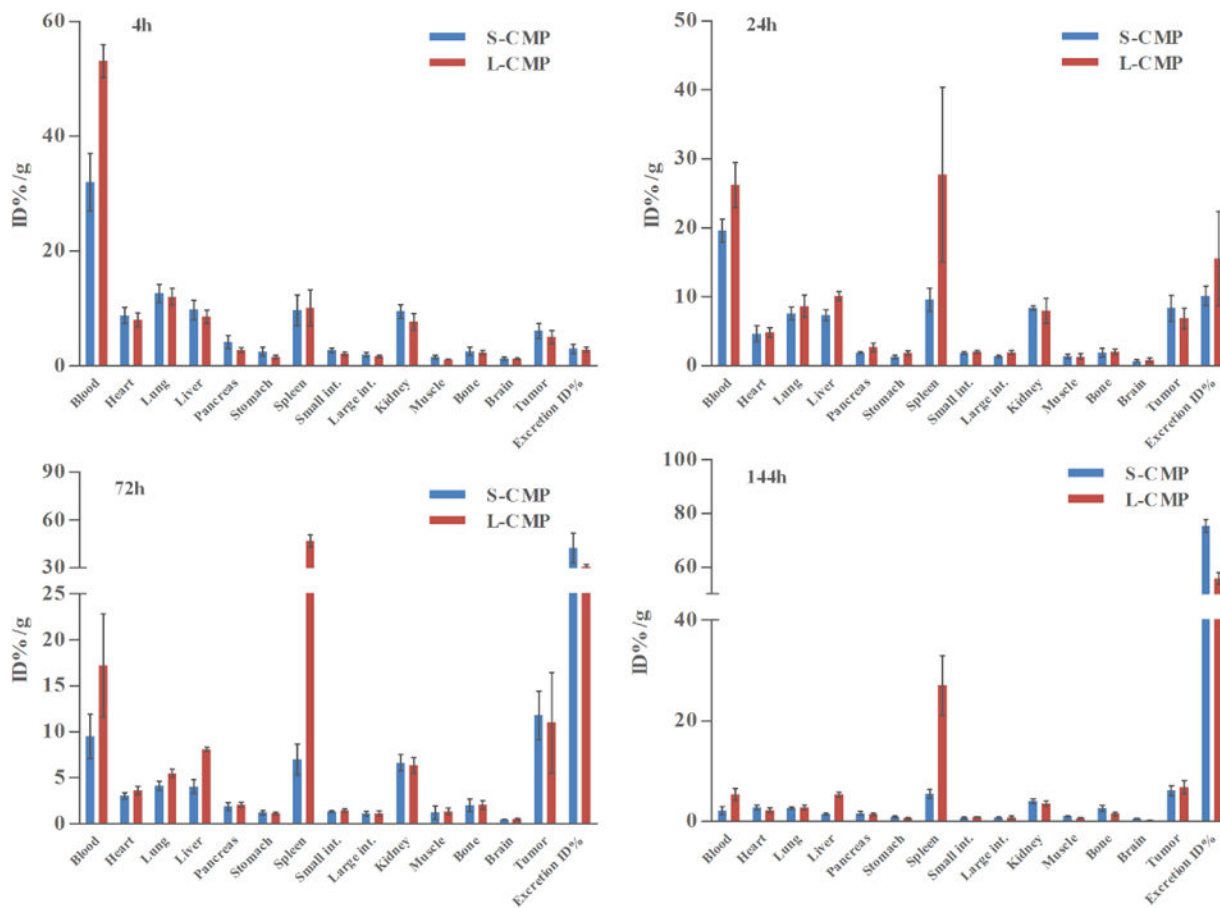Data are represented as mean ± SD. (n = 5).

Figure 7.
Biodistribution data of ^{177}Lu-labeled copolymers in a HPAC tumor bearing mouse model.
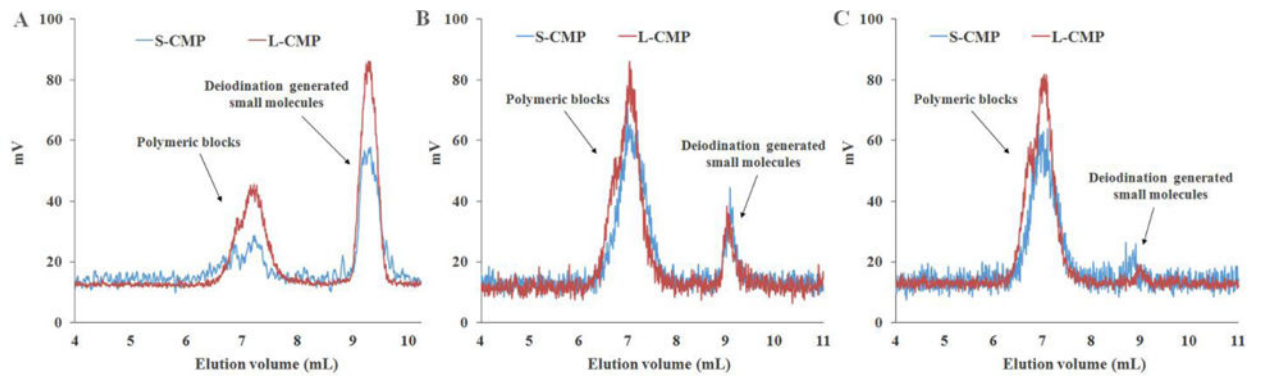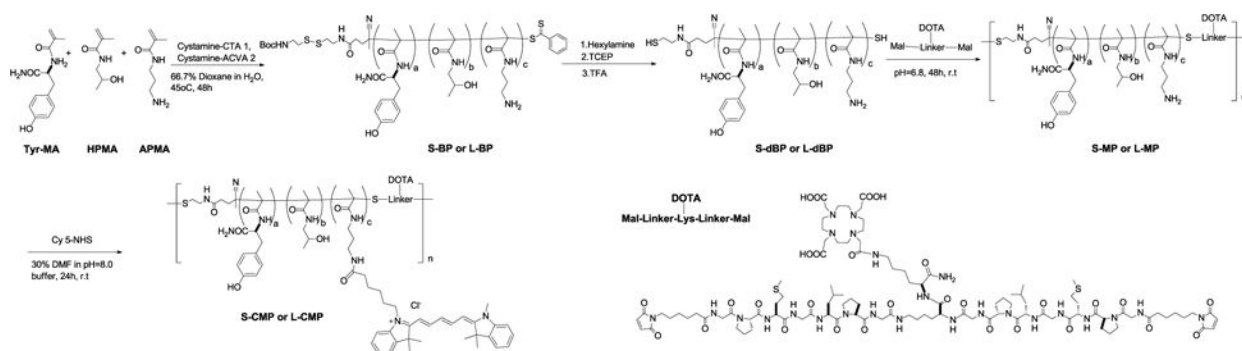Data are represented as mean ± SD. (n = 5).

Figure 8.
Radio-GPC profiles of CF-1 mice urine at 0 – 4 h (**A**), 4 – 72 h (**B**), and 72 – 144 h (**C**) after injection of 200 μCi of ^{125}I-labeled S-CMP and L-CMP.

Scheme 1.
Synthesis of S-CMP and L-CMP via RAFT polymerization and thiol-ene click chemistry.

Table 1

Characteristics of the synthesized HPMA copolymers

Copolymer	Mw (kDa)	PDI	Rh (nm)[a]	Tyrosine (Wt %)	Cy5 (Wt %)	Yield (%)
S-BP	17.4	1.03	2.85	–	–	87.6[b]
S-dBP	17.1	1.03	2.82	1.40	–	88.3[c]
S-MP	91.3	1.35	7.33	–	–	21.4[d]
S-CMP	92.5	1.34	7.21	–	0.31	91.7
L-BP	32.9	1.03	4.11	–	–	82.9[b]
L-dBP	31.1	1.05	4.02	1.36	–	85.2[c]
L-MP	139.3	1.37	9.76	–	–	17.3[d]
L-CMP	140.5	1.39	9.85	–	0.37	93.5

[a]Hydrodynamic radius detected by Viscotek TDAmax system

[b]Yield of RAFT polymerization

[c]Yield of reduction and deprotection by hexylamine and TCEP.

[d]Yield of copolymer chain extension after fractionation

Table 4

The $^{125}I/^{177}Lu$ ratios in tissues and excretion. The original $^{125}I/^{177}Lu$ ratios for S-CMP and L-CMP were 0.70 ± 0.02 and 0.73 ± 0.04 respectively.

Tissue	4 h		24 h		72 h		144 h	
	S-CMP	L-CMP	S-CMP	L-CMP	S-CMP	L-CMP	S-CMP	L-CMP
Blood	0.61 ± 0.05	0.66 ± 0.10	0.49 ± 0.06	0.63 ± 0.04	0.45 ± 0.03	0.62 ± 0.04	0.33 ± 0.08	0.61 ± 0.04
Liver	0.62 ± 0.06	0.85 ± 0.06	0.64 ± 0.03	0.80 ± 0.09	1.19 ± 0.02	1.04 ± 0.06	1.32 ± 0.12	1.53 ± 0.06
Spleen	0.54 ± 0.09	0.73 ± 0.04	0.58 ± 0.05	0.77 ± 0.07	0.82 ± 0.14	0.87 ± 0.06	1.16 ± 0.24	1.05 ± 0.09
Tumor	0.57 ± 0.11	0.87 ± 0.08	0.55 ± 0.03	0.73 ± 0.05	0.82 ± 0.02	0.88 ± 0.06	0.99 ± 0.09	1.13 ± 0.05
Excretion	1.54 ± 0.23	2.45 ± 0.15	1.10 ± 0.04	1.29 ± 0.19	0.74 ± 0.04	0.83 ± 0.05	0.48 ± 0.08	0.59 ± 0.03